JOURNAL OF AIRCRAFT
Vol. 42, No. 6, November–December 2005

# Engineering Notes

*ENGINEERING NOTES are short manuscripts describing new developments or important results of a preliminary nature. These Notes should not exceed 2500 words (where a figure or table counts as 200 words). Following informal review by the Editors, they may be published within a few months of the date of receipt. Style requirements are the same as for regular contributions (see inside back cover).*

## Undesired Equilibria of Self-Deploying Pneumatic Envelopes

Frank E. Baginski*
*George Washington University, Washington, D.C. 20052*
and
Willi W. Schur†
*Accomac, Virginia 17870*

### I. Introduction

THE advancement of materials and technology in thin lightweight films has generated great interest in deployable space structures for a variety of applications, including inflatable rovers, inflatable antennas, airbags to cushion landings, aerobots, and balloons. In this Note, we focus on two self-deploying structures: the zero-pressure natural shape balloon and the pumpkin shape superpressure balloon. The zero-pressure balloon has a long history of successful deployment. By contrast, the still experimental pumpkin shape superpressure balloon has a varied deployment history. Using a variational formulation and appropriate linear equality and inequality constraints, we explore the conditions that must be present for proper deployment and those that favor flawed deployment with the future aim to provide reliable design guidelines.

Zero-pressure natural shape (ZPNS) balloons have been flown successfully by NASA since the 1960s. The ZPNS balloon design is an axisymmetric shape that assumes that all of the loads are carried in the meridional direction and the hoopwise film stresses are zero.[1] The assumption of zero hoop stress is grossly violated by the real ZPNS balloon. However, the natural shape computations serve the shape finding process for the design purpose only, and even in the design of the ZPNS balloon, they serve this purpose well. Under normal circumstances, once a ZPNS balloon has been successfully launched, experience indicates that it will fully and properly deploy and attain float altitude.

The pumpkin balloon is radically different from the ZPNS balloon. By the suitable matching of material properties and the structural lack of fit between the load tendons and the skin, the strength requirement for the film can be made quite low. The details of the shape finding process for the theoretical doubly curved pumpkin gore are described in Ref. 1. This process yields a tubular surface $\mathcal{G}_F \in \mathbb{R}^3$ representing a typical inflated gore at float (Fig. 1b). Associated with $\mathcal{G}_F$ is a flat unstrained sheet of film, denoted by $G_F \in \mathbb{R}^2$ (Fig. 1a). $\mathcal{S}_F$ will denote a strained equilibrium configuration of the fundamental section of a pumpkin balloon (Fig. 1c). $G_F$ and $\mathcal{S}_F$ are discretized by triangular constant strain finite elements. Wrinkling in $\mathcal{S}_F$ is accounted for by using a relaxed strain energy formulation.

On 7 July 2002, a Phase IV-A ultra-long duration balloon (ULDB) deployed fully in flight 1580-PT, but failed due to a fabrication oversight. However, in Flight 517, its sister balloon designed to the same phase IV-A specifications, but with somewhat altered instructions to the fabricator, deployed 16 March 2003 into an undesired equilibrium state. The qualitative findings from the tests on small-scale balloons,[2] while giving some guidance, are clearly insufficient for guiding the design of pumpkin balloons. There is clearly a need for quantitative design thresholds that guarantee proper deployment. Indications exist that the larger the number of gores, the more likely it is that the balloon deploys improperly. The large number of gores in full-scale pumpkin balloons makes pursuing the goal of finding numerical thresholds via testing of physical models impractical. Analytical investigations are the only option. The variational approach with an optimization-based solution process that Baginski and Collier,[3] Baginski and Schur,[4] and Collier[5] have developed and applied to the analysis of balloon shapes shows promise in modeling undesired equilibria.

Whereas recent work in Refs. 6 and 7 indicates that an instability of the fully deployed cyclically symmetric pumpkin balloon may be the underlining reason for certain deployment problems, at this point, it is impossible to know with certainty what mechanism or sequence of events will trigger a flawed deployment. From our simulations presented here, we hope to gain a rough estimate of the forces that are needed to maintain an undesired equilibrium.

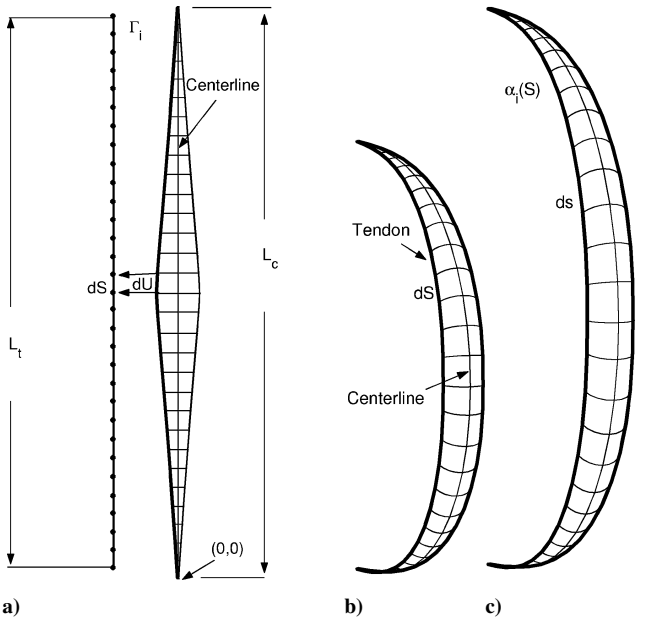


**Fig. 1 Pumpkin gore schematics: a) $G_F \in \mathbb{R}^2$, flat unstrained gore panel with load tendon, $L_t$ is unstrained tendon length and $L_c$ is unstrained length of the centerline of $G_F$; b) $\mathcal{G}_F \in \mathbb{R}^3$, theoretical pumpkin gore as determined by shape finding process (centerlines of $G_F$ and $\mathcal{G}_F$ identical in length); and c) $\mathcal{S}_F \in \mathbb{R}^3$, deformed pumpkin gore.**

Received 27 January 2005; presented as Paper 2005-1803 at the AIAA/ASME/ASCE/AHS/ASC 46th Structures, Structural Dynamics and Materials Conference, AIAA 6th Gossamer Spacecraft Forum, Austin, TX, 18–21 April 2005; revision received 22 May 2005; accepted for publication 9 June 2005. 

*Professor, Department of Mathematics; baginski@gwu.edu. Senior Member AIAA.
†(Retired), P.O. Box 698; pwschur@verizon.net. Senior Member AIAA.

## II. Finite Element Model

In this section, we summarize our approach of computing the equilibrium shape of a strained balloon. Variations of this model have been applied to ZPNS balloons[3,5] and to pumpkin balloons.[4,6] We refer to these references for details of our finite element model.

To achieve the proper tubular shape in a pumpkin balloon, tendon foreshortening is applied. The surface of the pumpkin balloon is modeled as a faceted surface, that is, a collection of triangles. We follow the approach of Pipkin[8] to account for wrinkling in the film. Pipkin's approach has been applied to pumpkin balloons[4,6] and to ZPNS balloons.[3,5]

A complete strained shape is denoted by $\mathcal{S} = \cup_{i=1}^{n_g} \mathcal{S}_i$. Each $\mathcal{S}_i$ is associated with a reference configuration $G_i$, which is isometric to $G_F$. The reference configuration associated with $\mathcal{S}$ is $\Omega = \cup_{i=1}^{n_g} G_i$. The gores are discretized by constant strain plane stress triangular finite elements. Adjacent gores are joined at their common edge. The tendons are modeled along these edges as rod elements that do not resist compression. The total potential energy $\mathcal{E}_t^*$ of a balloon configuration is

$$\mathcal{E}_T^* = \mathcal{E}_p + \mathcal{E}_f + \mathcal{E}_t + \mathcal{E}_{top} + S_t^* + S_f^* \tag{1}$$

where $\mathcal{E}_P$ is the hydrostatic pressure potential due to the lifting gas, $\mathcal{E}_f$ is the gravitational potential energy of the film, $\mathcal{E}_t$ is the gravitational potential energy of the load tendons, $\mathcal{E}_{\text{top}} = w_{\text{top}} z_{\text{top}}$ is the gravitational potential energy of the top fitting, $S_t^*$ is the relaxed tendon strain energy, and $S_f^*$ is the relaxed film strain energy. See Ref. 4 for definitions of these terms.

Let $\Gamma_i$ denote tendon $i$ in its reference configuration (Fig. 1a). The edge of a gore in the deformed configuration is given by a parametric curve $\alpha_i(S) \in \mathbb{R}^3$, where $S$ is arc length measured in $\Gamma_i$. A load tendon runs along the curve parametrized by $\alpha_i$.

The tendon length is determined by the $\mathcal{G}_F$ edge length as determined in the shape finding process. Let $L_t$ be the tendon length and let $0 \le S \le L_t$ denote arc length in $\Gamma_i$. By construction, the edge of $G_F$ is longer than $L_t$ (Fig. 1a). The lack of fit between these different lengths is accommodated by gathering the material along an edge of $G_F$ before attaching the tendon. If $U$ is arc length as measured along the edge of $G_F$, the local lack-of-fit function is $\tau(S) = \mathrm{d}U/\mathrm{d}S$, where, by construction, $\tau(S) > 1$ in a pumpkin balloon. No lack of fit is represented by $\tau = 1$.

To determine a strained balloon shape, we solve for $\mathcal{S} \in C$,

$$\text{minimize} \quad \mathcal{E}_T^*(\mathcal{S}), \qquad \text{subject to} \quad \boldsymbol{F}(\mathcal{S}) \le \boldsymbol{0} \tag{2}$$

where the components of $\boldsymbol{F}$ are derived from the symmetry conditions and other linear inequality and equality constraints. If a volume constraint is imposed, then

$$V(\mathcal{S}) - V_0 = 0 \tag{3}$$

is included as an equality constraint. $C$ denotes the class of feasible balloon shapes with appropriate boundary conditions. The differential pressure is in the form $-P(z) = bz + p_0$, and in an open system, $p_0$ is known. In a closed system, we assume $V = V_0$ is known. If $(\lambda, \mathcal{S})$ is a solution of problem (2) with volume constraint (3), then $\lambda$ can be interpreted as the change in the constant pressure that is needed to maintain the volume constraint, that is, $\lambda = \Delta p_0$ and $-p(z) = bz + p_0 + \Delta p_0$ at equilibrium. Here, the continuum problem is cast as an optimization problem. This approach is particularly well suited for the analysis of compliant structures.[3,4]

## III. Deployment Case Studies

In our case studies of large-scale pumpkin balloons, we use design parameters related to Flight 517. For the cleft simulations, we use a 6.6-m-diam test vehicle.

#### Estimating Restoring Forces when Not All Gores Deploy

The ZPNS design considered here is not one that has been flown by NASA and is used only for comparison purposes with the phase IV-A balloon. It is for this reason that we use the weight and stiffness of the ULDB tendons for the ZPNS case, even though a ZPNS design utilizes load tapes that are lighter and have significant slackness.

We begin by considering a number of cyclically symmetric strained balloons at full inflation. In our first case study, we consider the lay-flat gore pattern that was used in Flight 517. In the second case study, we consider a ZPNS design with similar lift capability as Flight 517.

For the pumpkin study, we varied the number of gores $N$ in the complete balloon. We let $\varphi(N)$ denote the wedge angle between the half-planes containing the z axis that bound a gore in a cyclically symmetric balloon in $\mathbb{R}^3$ with $N$ gores, that is, $\varphi(N) = 2\pi/N$. Initially, we assumed an open system with $p_0 = 170$ Pa and calculated the volume of the strained shape to be 0.585 million cubic meters. In the remaining scenarios, we considered a closed system, assuming $V_0 = 0.585$ mcm and then calculated $\Delta p_0$ for each $N$. In Table 1, we present a summary of our results on strained pumpkin balloons. For each entry in Table 1, we solved problem (2) and determined a cyclically symmetric strained equilibrium solution; maximum $\delta_1$ is the largest principal strain (corresponding to the hoop direction), $\hat{\delta}_1$ is the average of all hoop strains, and maximum $\mu_1$ is the largest principal stress resultant. The last column in Table 1 contains the maximum radius and height of the strained balloon. From Table 1, it is obvious that there is little change in the film stress resultants when the number of gores is varied by $\pm 4$. When eight gores are removed, there is a 43% increase in the maximum film stress resultant.

In Table 2, we present similar results for a ZPNS balloon. Because a zero-pressure balloon is open at its base and $p_0 = 0$, we do not enforce a volume constraint. In Table 2, we include maximum $\mu_i$, maximum $\delta_i$, and $\hat{\delta}_i$. As $N$ decreases, we find a dramatic change in film strains and principal stress resultants. In Table 2, we see the maximum film stress resultant increases to a total of 700% when four gores are removed.

The results in Tables 1 and 2 suggest how a balloon may respond to a situation in which some mechanism is inhibiting deployment. Table 1 suggests that if a set of four gores in a pumpkin cleft are unable to deploy and 286 fully deploy, the film in the region exterior

**Table 1 Pumpkin parametric studies**

| $N$ | $\varphi(N)$, deg | $\mathcal{E}_T^*$, MJ | Maximum $\delta_1$, m/m | $\hat{\delta}_1$, m/m | Maximum $\mu_1$, N/m | $\Delta P_0$, pa | $V/N$, $m^3$ | (Maximum $r$, maximum $z$), m,m |
|---|---|---|---|---|---|---|---|---|
| 294 | 1.22 | −99.09 | 0.0110 | 0.0061 | 169 | 0.4433 | 1993 | (59.81, 72.43) |
| 290 | 1.24 | −99.07 | 0.0112 | 0.0065 | 173 | 0.0000 | 2020 | (59.80, 72.47) |
| 286 | 1.26 | −99.06 | 0.0114 | 0.0071 | 176 | 0.6946 | 2049 | (59.79, 72.52) |
| 282 | 1.28 | −99.03 | 0.0117 | 0.0085 | 252 | 1.8416 | 2078 | (59.78, 72.58) |

**Table 2 ZPNS parametric studies**

| $N$ | $\varphi(N)$, deg | $\mathcal{E}_T^*$, MJ | Maximum $\delta_1$, m/m | $\hat{\delta}_1$, m/m | Maximum $\mu_i$, N/m | $V/N$, $m^3$ | (Maximum $r$, maximum $z$), m,m |
|---|---|---|---|---|---|---|---|
| 294 | 1.22 | −1.651 | 0.00277 | 0.00115 | 50 | 1939 | (55.50, 97.37) |
| 290 | 1.24 | −1.664 | 0.00321 | 0.00149 | 62 | 1962 | (55.51, 97.35) |
| 286 | 1.26 | −1.666 | 0.00621 | 0.00192 | 434 | 1976 | (55.19, 99.25) |

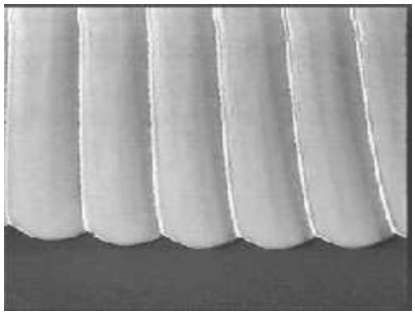

**a) Proper deployment**

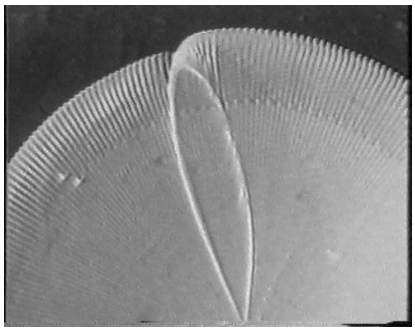

**b) Flight 517 Cleft**

**Fig. 2 Snapshots from ULDB pumpkin flights.**

to the cleft would respond with a reaction force that is only moderately greater than nominal. This is in sharp contrast to the case of a ZPNS balloon, where the scenario of merely four undeployed gores would generate very large reaction forces.

#### Numerical Simulations of Clefts

Even though it is not possible to give a precise description as to how the cleft evolved in Flight 517, photographic evidence supports the view that the cleft formed in the launch spool was maintained through the ascent phase and remained once the balloon attained float altitude (Fig. 2b). A closeup of a properly deployed pumpkin balloon is shown in Fig. 2a. In Flight 517, it appears that several gores that make up the cleft were drawn inboard while the majority of the remaining gores outside the cleft assembly were fully deployed. A careful examination of the photographs from Flight 517 indicates that at least eight gores participated in the cleft formation.

To analyze a vehicle with many gores and at least one asymmetric cleft assembly, and to keep the number of degrees of freedom manageable, we will make a few simplifying assumptions. We will break the symmetry of the desired cyclic shape by modifying boundary conditions and adding fictitious internal rope forces. The ropes are introduced for the sole purpose of inducing a cleft.

For demonstration purposes, we suppose that the properly designed test article has 96 gores, $r_B = 0.11$ m, and a diameter of about 6.6 m. To increase the likelihood that a cleft will form, we add 4 gores bringing the total number of gores to 100. We focus on a collection of eight gores, consisting of two fully deployed gores bounding six contiguous gores that form the cleft assembly. We will consider two approaches to induce a cleft:

*Case 1* We introduce two internal pulley systems. In one system, a uniformly tensioned rope loops through pulleys located on the endplates and selected interior nodes along some tendon. Its tension is increased by winching in the rope. A second rope system is a mirror image of the first. See Fig. 3a, where we present an equilibrium configuration with two opposing clefts. The two symmetric cleft assemblies consist of a total of 12 gores. The remaining 88 gores are uniformly deployed. In Fig. 3b, we present an external view of eight contiguous gores in a fully deployed configuration without cleft-inducing ropes. In Fig. 3c, an outside view of the simulated cleft feature is presented.

*Case 2* A uniformly tensioned rope segment connects each of 20 selected nodes on 1 tendon to a corresponding node and tendon on

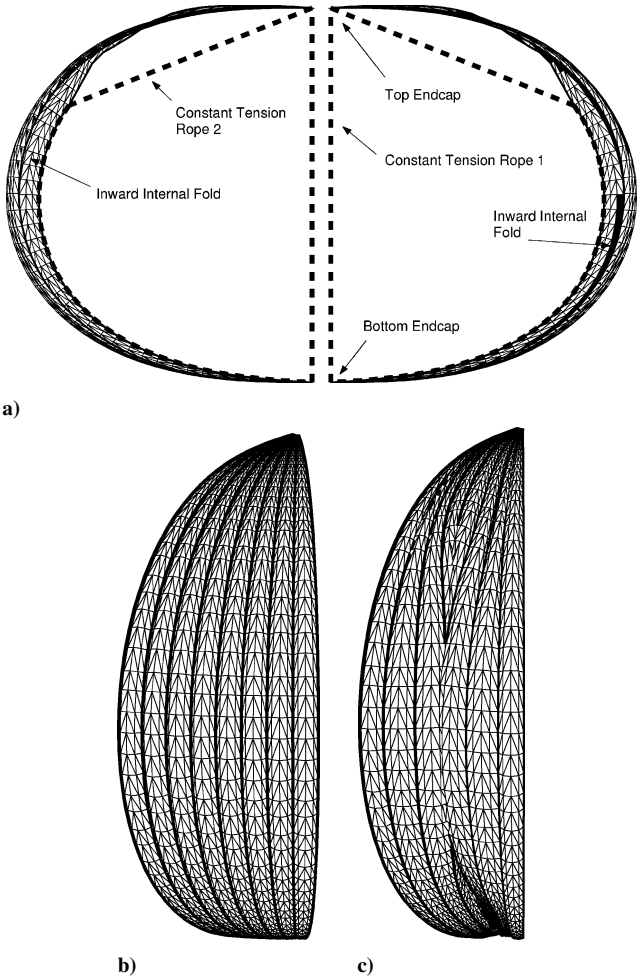


**Fig. 3 Simulating clefts: a) two internal pulley systems located inside balloon where rope tension of 30 N is needed to maintain the cleft (case 1); b) exterior view of eight fully deployed gores; and c) exterior view of simulated cleft.**

the opposite side of the balloon. The ropes span the interior of the balloon. Although the cleft inducing mechanism is different in this case, the external view of the cleft was very similar to case 1.

In each case, we add an appropriate rope strain energy terms in $\mathcal{E}_T^*$ to include the contributions of cleft inducing ropes. Let $\theta_1$ denote the wedge angle defined by the half-planes that that bound a uniformly deployed gore. Let $\theta_2$ denote the wedge angle of a cleft assembly. There are 88 gores that are fully deployed and two 6-gore clefts (each of angle $\theta_2$), so that $2\theta_2 = 2\pi - 88\theta_1$. Roughly speaking, tensioning the cleft inducing ropes will increase $\theta_1$ and decrease $\theta_2$.

*Remark:* Strictly speaking, boundary conditions in our cleft studies are not without error. It is unlikely that the edge forces acting on an edge of a uniformly deployed gore are the same as those acting on the edge of a cleft. However, after examining our final results, we find they are sufficiently consistent for the purposes of this exploratory work.

In case 1, the maximum tension in the constraining ropes is approximately 30 N. In case 2, we find the maximum rope tension is approximately 4 N. The internal ropes merely serve to help organize excess material. The cleft simulated in Fig. 3 is one way that the excess balloon film can distribute itself when an undesired equilibrium shape is possible.

## IV. Conclusions

We compared pumpkin and ZPNS strained balloon configurations related to the Flight 517 design. We found that in scenarios where the balloon is not fully deployed, the restoring forces that would be generated by the film in the deployed region of the balloon would be much higher in a ZPNS balloon than in a pumpkin balloon. Our

results on balloons with clefts provide evidence that we can model scenarios that are representative of self-locking balloon shapes and undesired equilibria. Fictitious forces that were added to maintain a cleft in our test scenarios were found to be relatively small. The natural step would be to build a test vehicle and experimentally reproduce a shape predicted by our finite element model. The availability of a test vehicle would also allow us to probe the phenomena of tendon locking.

## Acknowledgments

The first author was supported in part by NASA Grant NAG5-5353. The authors thank NASA Balloon Program Office for the use of photographs included in this Note.

## References

[1]Baginski, F., "On the Design and Analysis of Inflated Membranes: Natural and Pumpkin Shaped Balloons," *SIAM Journal on Applied Mathematics*, Vol. 65, No. 3, 2005, pp. 838–857.

[2]Schur, W. W., and Jenkins, C. H., "Deployment Destiny, Stable Equilibria, and the Implications for Gossamer Design," AIAA Paper 2002-1205, April 2002.

[3]Baginski, F., and Collier, W., "Modeling the Shapes of Constrained Partially Inflated High Altitude Balloons," *AIAA Journal*, Vol. 39, No. 9, 2001, pp. 1662–1672; errata, *AIAA Journal*, Vol. 40, No. 9, 2002, p. 1253.

[4]Baginski, F., and Schur, W., "Structural Analysis of Pneumatic Envelopes: A Variational Formulation and Optimization-Based Solution Process," *AIAA Journal*, Vol. 41, No. 2, 2003, pp. 304–311.

[5]Collier, W. G., "Estimating Stresses in a Partially Inflated High Altitude Balloon Using a Relaxed Energy," *Quarterly of Applied Mathematics*, Vol. 61, No. 1, 2003, pp. 17–40.

[6]Baginski, F., Brakke, K., and Schur, W., "Stability, Clefting and Other Issues Related to Undesired Equilibria in Large Pumpkin Balloons," AIAA Paper 2005-1803, April 2005.

[7]Baginski, F., Brakke, K., and Schur, W., "Cleft Formation in Pumpkin Balloons," *Advances in Space Research* (to be published).

[8]Pipkin, A. C., "Relaxed Energy Densities for Large Deformations of Membranes," *Journal of Applied Mathematics*, Vol. 52, No. 3, 1994, pp. 297–308.